Bull Earthquake Eng (2012) 10:1321–1337
DOI 10.1007/s10518-012-9345-z

Variations of the specific barrier model—part II: effect of isochron distributions

Benedikt Halldorsson · Apostolos S. Papageorgiou

Received: 23 May 2011 / Accepted: 19 February 2012 / Published online: 16 March 2012

Abstract The specific barrier model (SBM) is a particular case of a composite earthquake source model where the seismic moment is distributed in a deterministic manner on a rectangular fault plane on the basis of moment and area constraints. It is assumed that the fault surface is composed of an aggregate of subevents of equal diameter, the 'barrier interval'. Furthermore, the subevents are assumed to rupture randomly and statistically independent of one another as the rupture front sweeps the fault plane. In the formulation of the far-field source spectrum of the SBM the 'arrival time' of the seismic radiation emitted by each subevent is specified via a probability density function (PDF). In the SBM the subevents are assumed to be of equal sizes (an assumption relaxed in a companion paper, referred to as Part I) and the PDF of 'arrival times' is assumed to be uniform. In this study we investigate the effects of different PDFs of 'arrival times' on the far-field source spectrum of the SBM. Different PDFs of 'arrival times' affect the source spectra primarily at the intermediate frequency range (between the first and second corner frequencies). Such effects become more pronounced as the earthquake magnitude increases. The far-field spectrum of seismic energy observed/recorded at a site depends on the location of the site relative to the causative fault plane, the location of rupture initiation (hypocenter) and the onset times of the rupturing subevents. All the above factors are effectively taken into account by the 'isochrons', which vary with source-site geometry. We investigate the selection of the appropriate PDF of seismic energy arrival times at a given site by computing isochrons for a grid of stations surrounding the earthquake fault, represented by the SBM. We show that only for stations located in a

B. Halldorsson (✉)
Earthquake Engineering Research Centre, University of Iceland, Austurvegur 2A, 800 Selfoss, Iceland
e-mail: skykkur@hi.is

B. Halldorsson
Faculty of Civil and Environmental Engineering, School of Engineering and Natural Sciences, University of Iceland, Hjarðarhagi 2-6, 107 Reykjavík, Iceland

A. S. Papageorgiou
Department of Civil Engineering, University of Patras, 26500 Patras, Greece
e-mail: papaga@upatras.gr

direction normal to the fault plane is the assumption of uniform PDF of 'arrival times' valid. At other sites non-uniform PDFs of 'arrival times' are observed. We identify and categorize the prevalent types of PDFs by directivity (forward vs. backward vs. neutral) and source-site distance (near-fault vs. far-field), show examples in which we group the stations accordingly. We investigate the effects of the different PDF-groups on the SBM source spectrum. Selection of the appropriate PDF for a given source-site configuration when simulating strong ground motions using the SBM in the context of the stochastic method is expected to yield more self-consistent, and physically realistic simulations.

Keywords Earthquake · Specific barrier model · Far-field source spectra · Isochron · Directivity

1 Introduction

In earthquake prone regions where strong-motion data is scarce, the reliability of strong ground motion simulations depends heavily on realistic source, path and site models. Due to the inherent uncertainty and randomness of earthquake processes and crustal heterogeneities, reducing the standard error associated with empirical attenuation relationships has proven difficult (Trifunac and Brune 1970; Douglas 2010). Additionally, such relationships are strictly speaking not valid outside the range which the data define. Therefore, it is strongly recommended to seek physically realistic models, especially of the earthquake source, for ground motion simulation. The specific barrier model (SBM) is such a model in which a complete, yet parsimonious and self-consistent description is provided of the faulting processes that are responsible for the generation of high-frequency waves ($\gtrsim 1$ Hz). It has been successfully applied in the context of the stochastic modeling approach, using random vibration theory, on the basis of the closed-form expression of the far-field source spectrum of the SBM (Halldorsson and Papageorgiou 2005). Furthermore, the model is especially well suited for physically realistic, fast and efficient strong-motion simulations, both in the near-fault as well as far-field regions of a finite earthquake source (Mavroeidis and Papageorgiou 2003; Halldorsson et al. 2007, 2011).

In a companion paper (Part I) of the present study we revisit the SBM as a particular case of a composite seismic source model according to which the seismic moment is distributed in a deterministic manner on the fault plane on the basis of moment and area constraints (Halldorsson and Papageorgiou 2012). Namely, in formulating the model it is assumed that a rectangular fault surface is composed of an aggregate of subevents of equal diameter, the "barrier interval". Furthermore, the subevents are assumed to rupture randomly and statistically independent of one another as the rupture front sweeps the fault plane. In the aforementioned study basic assumptions regarding subevent size of the SBM were relaxed. By allowing subevent sizes to vary according to various prescribed probability density functions (PDF), closed form expressions of the corresponding far-field source spectra of the composite source were derived. It was shown that high-frequency spectral asymptotes corresponding to different types of size-distributions and for realistic size-ranges do not differ significantly from those associated with the SBM, for a constant local stress drop. Furthermore, the difference is likely to be less than the expected uncertainty associated with local stress drop values determined from strong-motion data. Thus, despite its simplifying assumptions, the SBM appears to be the most simple, yet effective, way to capture the essential characteristics of a composite seismic source. This is especially advantageous for consistent strong-motion

modeling in the 'near-fault', as well as in the 'far-field' region for earthquake engineering applications (Mavroeidis and Papageorgiou 2003; Halldorsson et al. 2007, 2011).

While in Part I we relaxed assumptions regarding the size distribution of the subevent population, we kept the assumption that the 'arrival times' of the seismic radiation emitted by the subevents were uniformly distributed over the time window of motion at a recording station (observation point). In the present study (Part II) however, we keep the assumption regarding subevent size distribution of the SBM (i.e., all subevents have the same size) but investigate the effects of various distributions of 'arrival times' at a station. [Parenthetically we note that we use the term 'arrival times' following Davenport (1970), while for the same concept, Wennerberg (1990), used the term 'delay times' or 'lags'.] The 'arrival times' vary with source-site geometry, and this variation is effectively captured by the isochrons on the fault plane (Spudich and Frazer 1984). We consider the arrival times to be a random variable because earthquake sources are highly complex (e.g., generally, the rupture front is not circular, the subevents are not perfect circles with perfectly defined centers, and subevents are not uniformly distributed on the fault plane, etc.). The random 'arrival times' can therefore also be viewed as means to effectively account for such uncertainties in the modeling. Thus, we investigate the effect of variations of the PDF of 'arrival times' on the seismic radiation received at a given site by computing isochrons on a vertical fault plane of the SBM for each station of a hypothetical grid of stations. We show that, for stations located in the far-field and in a direction normal to the fault plane, the assumption of uniform PDF of 'arrival times' is valid. At other sites non-uniform PDFs of 'arrival times' are generally observed. We identify and categorize the prevalent groups of PDFs by directivity (forward vs. backward vs. neutral) and proximity to the fault plane (near-fault vs. far-field). As the PDF of 'arrival times' enters directly into the formulation of the far-field spectrum radiated from a composite source, the SBM source spectrum varies depending on the source-site geometry. Thus, selecting the appropriate PDF for a given source-site configuration when simulating strong ground motions using the SBM in the stochastic method is expected to enhance the physical basis of such simulations.

2 The specific barrier model

The specific barrier model was introduced and developed by Papageorgiou and Aki (1983a,b) for the quantitative description of heterogeneous rupture (see also Papageorgiou and Aki 1985; Aki and Papageorgiou 1988; Papageorgiou 1988, 2003). According to the SBM the seismic fault may be visualized as a rectangular fault of length L and width W which consists of an aggregate of N circular subevents (shear cracks) of equal diameter, $2\rho_o$ (the "barrier interval") on which a uniform stress drop, $\Delta\sigma_L$, (referred to as the "local stress drop") takes place and spreads radially with constant rupture velocity v (see Fig. 1a). The seismic moment of each subevent is

$$M_{o_i} = \frac{16}{7}\Delta\sigma_L \rho_o^3 \tag{1}$$

(Eshelby 1957; Keilis-Borok 1959) and is released when subevent rupture is triggered by the sweeping (with velocity V) rupture front. An analytical expression of the far-field radiation emitted by a circular crack has been derived by Sato and Hirasawa (1973) and is used in the SBM to represent the radiation of the subevents. For simplicity, Papageorgiou (1988) approximated the far-field source displacement spectrum of each subevent by an "*ω-square*" spectrum (Aki 1967) as

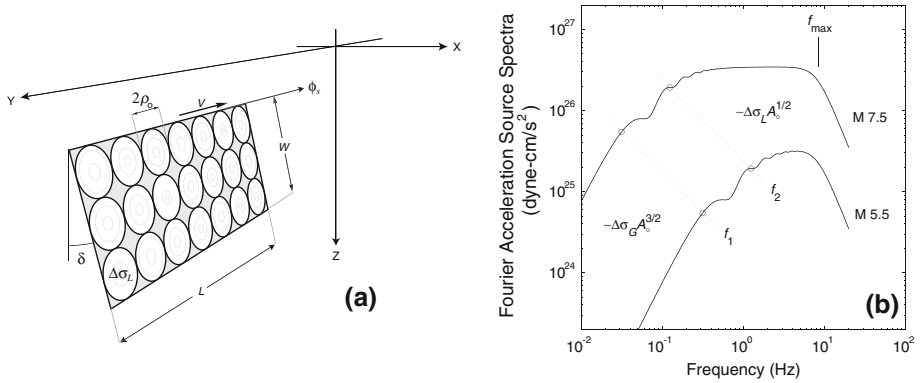

Fig. 1 **a** A schematic view of the SBM representing the earthquake fault consisting of equal-size subevents arranged in a non-overlapping manner on the fault plane. Subevent rupture starts at the center of each crack associated with a 'local stress drop' $\Delta\sigma_L$ and spreads radially outwards (the rupture fronts at successive time instants are denoted by *the light circles*) until it is arrested by the barriers, denoted by *the shaded area* between the cracks. **b** A schematic plot of the earthquake source spectra of the SBM for two magnitudes, M_w5.5 and 7.5, showing the loci of the first and second corner frequencies, and the effects of $f_{\max}$. Also shown are the dependencies of the spectral levels below and above the first and second corner frequencies, respectively, on stress drops and main source area A_o (from Part I)

$$\tilde{\dot{M}}_{o_i}(f) = \frac{M_{o_i}}{1 + (f/f_2)^2} \tag{2}$$

where f_2 is the "patch" corner frequency related to the size of the subevent, given by

$$f_2 = \frac{C_s \beta}{2\pi\rho_o} \tag{3}$$

averaged over the focal sphere, and C_s is model dependent and an implicit function of the ratio v/β [$1.72 \leq C_s \leq 1.85$ for $0.7 \leq v/\beta \leq 0.9$] for the symmetric circular crack (Sato and Hirasawa 1973; Aki and Richards 1980), where β is the shear wave velocity in the vicinity of the source.

The low-frequency radiation from the subevent population is summed up coherently and is proportional to the seismic moment of the main event $M_o = M_{o_i} N$. On the other hand, the high-frequency radiation from the subevents is summed up incoherently in the far-field region (Papageorgiou and Aki 1983a). The far-field spectrum of the SBM was originally presented by Papageorgiou and Aki (1985) who combined the then available description of the high frequency radiation to that of the low frequency. In a later publication, Papageorgiou (1988), exploiting a closed form expression of the far-field radiation of a composite source derived by Joyner and Boore (1986), presented a closed form expression of the far-field radiation of the SBM (for a comprehensive discussion see Part I). Subsequently, Halldorsson and Papageorgiou (2005) modified slightly the abovementioned closed form expression by introducing a high-frequency 'source complexity factor', ζ, into the expression, as follows

$$S(M_o, f, \zeta) = \sqrt{N\zeta + N(N-\zeta)\left(\frac{\sin(\pi f T_0)}{\pi f T_0}\right)^2} (2\pi f)^2 \tilde{\dot{M}}_{o_i}(f) \tag{4}$$

The high-frequency complexity factor is required to account for the observed high-frequency deviation from self-similar source spectral scaling of earthquakes in interplate tectonic regimes [$\zeta = 10^{2\eta}$, $\eta = s_m (M_w - M_{cr})$ where $s_m = -0.12$ and $M_{cr} = 6.35$)]. For

more details the reader is referred to Halldorsson and Papageorgiou (2005) and references therein.

The parameter T_0 is the duration of pulse-train (emitted by the subevents as they rupture) that is received at a station. An estimate of T_0 may be obtained by calculating the duration of faulting of the composite source, which is inversely proportional to the (first) corner frequency of the source spectrum, $T_0 = \tilde{C}/f_\circ$, where $\tilde{C}$ is a model dependent constant (e.g., Silver 1983). For simplicity and convenience we proceed by assuming geometric and kinematic similarity of the main event and its subevents. On this basis the first corner frequency becomes

$$f_\circ = \frac{C_s \beta}{2\pi R_\circ} \tag{5}$$

where $R_\circ$ is the radius of an 'equivalent' circular main source of area $A_\circ = LW$ with seismic moment

$$M_\circ = \frac{16}{7} \Delta\sigma_G R_\circ^3 \tag{6}$$

where $\Delta\sigma_G$ is referred to as the "global stress drop". Following Papageorgiou (1988) we set $\tilde{C} = C_s/4$ so that the first corner frequency of the SBM conforms with the locus of Gusev (1983) corner frequencies of empirical source spectra. This in turn implies that the corresponding duration of rupture is

$$T_0 = \frac{C_s}{4 f_\circ} \tag{7}$$

We acknowledge that one could adopt a more sophisticated relation of the (first) corner frequency to the characteristic dimension(s) of the main event, however, it should be pointed out that the above simplification has no significant effect on the overall source spectrum of the SBM, while it allows for the following concise expressions relating the barrier interval to the number of subevents (Eqs. 27 & 28 of Part I)

$$2\rho_\circ = \frac{4}{\pi} \frac{\Delta\sigma_G}{\Delta\sigma_L} 2R_\circ \tag{8}$$

$$N = \left(\frac{\pi}{4}\right)^3 \left(\frac{\Delta\sigma_L}{\Delta\sigma_G}\right)^2 \tag{9}$$

Therefore, in order to construct the seismic spectrum (see Fig. 1b) of the SBM for an earthquake event of a given seismic moment, one needs the values of the global and local stress drops and the expressions (8) & (9) given above. We note that Halldorsson and Papageorgiou (2005), in re-calibrating the SBM, have provided values for (*i*) the global stress drop $\Delta\sigma_G$ based on data in the published literature, and (*ii*) the local stress drop $\Delta\sigma_L$ from inversion to strong-motion data for three different tectonic regions (see also Foster et al. 2012).

3 Distributions of pulse 'arrival times' and effects on far-field source spectra

The expectation of the squared absolute value of the Fourier amplitude of the far-field spectrum of a composite source that consists of subevents of random sizes is expressed as (Joyner and Boore 1986)

$$E\left[|S(\omega)|^2\right] = N \cdot E\left[|S_R(\omega, R)|^2\right] + N(N-1) \cdot \left|\tilde{f}_T(\omega)\right|^2 \cdot \{E[|S_R(\omega, R)|]\}^2 \quad (10)$$

where $S_R(\omega, R)$ is the subevent seismic spectrum and $\tilde{f}_T(\omega)$ is the *'characteristic function'* of the random variable T, which represents the arrival time (at a station/observation point) of the radiation emitted by a subevent rupture (Joyner and Boore 1986; Halldorsson and Papageorgiou 2012). [Parenthetically we mention that Eq. (10) is in essence a statement of Campbell's theorem (see Rice 1944, 1945; Middleton 1960; and Lin 1967; and references therein; see also Lin and Cai 1995) for a pulse-train of finite duration.] In the formulation of the far-field spectrum of the SBM in Eq. (4), we substitute the subevent seismic spectrum from Eq. (2) into Eq. (10) and calculate the expectations that appear on the right hand side. In the original studies (Joyner and Boore 1986; Papageorgiou 1988) the PDF of 'arrival times' was assumed to be constant over the time interval 0 to T_0. In this case the PDF is expressed as

$$f_T(t) = \frac{1}{T_0}, \quad t \in [0; T_0] \quad (11)$$

The Fourier transform of $f_T(t)$ is denoted by $\tilde{f}_T(\omega)$, and is referred to as the 'characteristic function' of the R.V. T (Papoulis 1965). The squared amplitude of the characteristic function, corresponding to the PDF in Eq. (11), is

$$\left|\tilde{f}_T(\omega)\right|^2 = \sin^2\left(\frac{\omega T_0}{2}\right) \Big/ \left(\frac{\omega T_0}{2}\right)^2 \quad (12)$$

where $\omega = 2\pi f$ is the circular frequency. Substituting this expression into Eq. (10) and taking the square root i.e., $|S_C(\omega)| = \sqrt{E\left[|S(\omega)|^2\right]}$, we obtain the Fourier amplitude of the far-field source spectrum of the SBM that appears in Eq. (4) (apart from the high-frequency complexity factor). For more information the reader is referred to Part I and references therein (Halldorsson and Papageorgiou 2012).

A characteristic of Eq. (12) is that it decays proportionally to ω^{-2} and has spectral "holes" i.e., periodic set of zeros at $\omega = p(2\pi/T_0)$ where p is a positive integer (Joyner and Boore 1986; Wyss and Brune 1967). Furthermore, being the characteristic function of the R.V. T, its limits as f approaches 0 and ∞ are one and zero, respectively (Papoulis 1965). It follows that the low-frequency limit of the source displacement spectrum in Eq. (10) is equal to the cumulative seismic moment M_o while the high-frequency limit of the source acceleration spectrum is $\sim \sqrt{N} f_2^2 M_{o_i}$ (for self-similar scaling $\eta = 0$). At low-frequencies therefore, energy is summed coherently (conserving the moment), while in the high-frequency range, the radiated spectra of the individual subevents are summed up incoherently. Consequently, in the high frequency range spectral amplitudes are proportional to the square root of the number of subevents (Papageorgiou and Aki 1983a). The general role of $f_T(t)$ on the source spectrum of the SBM can thus be investigated in terms of Eqs. (10) and (12). This is illustrated in Fig. 2a showing how the displacement spectrum expressed by Eq. (10) is the summation of two dominant (at different ends of the spectrum) terms: at long periods, the dominant term is $N(N-1) \cdot \left|\tilde{f}_T(\omega)\right|^2 \cdot \{E[|S_R(\omega, R)|]\}^2$, while at high frequencies spectral amplitudes are controlled by the term $N \cdot E\left[|S_R(\omega, R)|^2\right]$. In the same figure one can observe also that the shape of $|\tilde{f}_T(\omega)|^2$ affects the spectra primarily in the intermediate frequency range (f_1 to f_2). In general therefore, the role of $|\tilde{f}_T(\omega)|^2$ is essentially that of a transition "agent" between

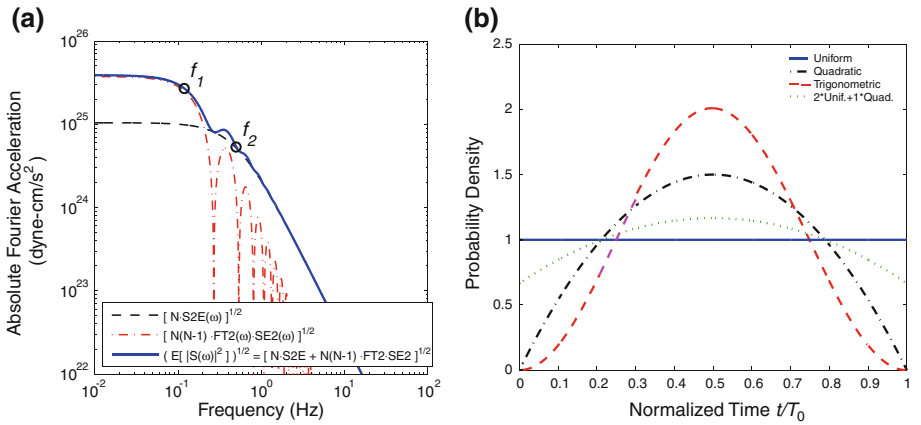

Fig. 2 **a** The SBM displacement spectrum for a M_w6.5 event with $\Delta\sigma_G = 30$ bar and $\Delta\sigma_L = 161$ bar. *The solid line* is the aggregate seismic spectrum and *the dashed* and *dot-dashed lines* indicate the contribution of the first and second terms, respectively, on the right hand side of Eq. (10) (from Part I). **b** The constant PDF of subevent rupture times (normalized by T_0) displayed along with three hypothetical PDFs of quadratic, trigonometric and combination of uniform and quadratic terms, respectively

the coherent and incoherent spectral ranges (see e.g., Frankel 1991), while the number of subevents determine the low- and high-frequency asymptotes (see Part I).

While the uniform distribution of 'arrival times' appears to be both a physically reasonable and simple assumption, other distributions may of course be assumed. [For example, Wennerberg 1990 selected a $\tilde{f}_T(\omega)$ that was proportional to the spectral ratio of the source spectrum and the main event to that of the subevent. However, his choice of $\tilde{f}_T(\omega)$ does not satisfy the requirement that a characteristic function should satisfy, i.e. $\lim_{\omega\to\infty} \tilde{f}_T(\omega) = 0$, and therefore his selection of $\tilde{f}_T(\omega)$ does not correspond to any PDF.] In the present work, we start by postulating a PDF $f_T(t)$ (the selected $f_T(t)$ may be motivated by empirical observations as it will become evident below, and it must always satisfy the conditions of 'nonnegativeness' $f_T(t) \geq 0$ and 'unit area' $\int_{-\infty}^{+\infty} f_T(t)\,dt = 1$) and we compute in a straightforward way the corresponding $\tilde{f}_T(\omega)$. As a simple exercise we postulated a quadratic, a trigonometric, and a combination of uniform and quadratic PDFs, shown in Fig. 2b. The respective $|\tilde{f}_T(\omega)|^2$ are shown in Fig. 3i and in all cases, the low- and high-frequency limits are 0 and 1, respectively as expected, but different corner frequencies and spectral falloff rates are observed. The effects that these functions have on the SBM source spectrum is shown in Fig. 3ii for the case of a M_w 5.8 interplate event ($\Delta\sigma_G = 30$ bar, $\Delta\sigma_L = 161$ bar). The effects are seen to be dominated by the different values of the corner frequency of the $|\tilde{f}_T(\omega)|^2$-functions in Fig. 3i. The different assumptions of PDFs of 'arrival times' in effect change the apparent value of the lower corner frequency of the source spectrum, as well as the intermediate slope between the lower and upper corner frequencies of the composite event. In any case, the effects are evident and warrant further consideration.

4 Distributions of pulse 'arrival times' and their physical manifestations

Simulation of earthquake ground motion using the SBM relies (at least in part) on the observed fact (e.g. Trifunac and Brune 1970; Wyss and Brune 1967; Vallée and Bouchon 2004) that earthquake seismograms can be, reasonably well, simulated by using a relatively small

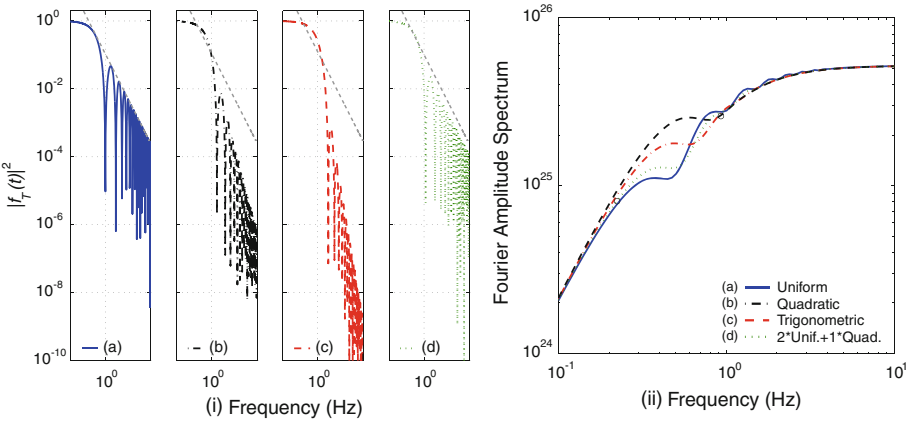

Fig. 3 **i** *The squared* FAS of the PDFs $f_T\ (t)$ of rupture times shown in Fig. 2b i.e., plots (a)–(d) correspond to the uniform, quadratic, trigonometric, and the combined uniform and quadratic PDFs, respectively. **ii** The corresponding SBM source acceleration spectra. *The dashed gray lines* in (**i**) show the spectral slope of the FAS of the uniform PDF

number of resolvable, energetically significant subevents. The subevents of the SBM are assumed to rupture statistically independently of one another as the expanding rupture front sweeps the fault plane (Papageorgiou and Aki 1983a). Such a rupture process had been anticipated by Housner (1947, 1955). Figure 4a, b shows on the left the fault planes of a $M_w 6.5$ earthquake event modeled using the SBM. An expanding circular rupture front, originating at the hypocenter (located at $0.8W$ downdip and denoted by a star), sweeps the fault plane with constant sweeping rupture velocity $V = 0.75\beta$ (unilaterally in Fig. 4a and bilaterally in Fig. 4b). The solid lines denote the rupture front at successive time instants (contour interval $\Delta t = 1.5$ s) over the rupture duration. Subevent rupture commences when the rupture front reaches its center (Halldorsson et al. 2011). We refer to the above time instant as the subevent 'onset' time.

Let us consider now a line which is normal to the fault plane at its hypocenter. Consider now a station located on this line and at a very large distance (ideally infinite) from the fault plane. For such a station, the lines representing the expanding rupture front in Fig. 4a, b coincide also with the 'isochrons' corresponding to the station. [We remind the reader that an 'isochron' (corresponding to a station) is the locus of points on the fault plane the (instantaneous/impulsive) radiations of which reach the station simultaneously.] Therefore, it is evident that for such a station the sequence of 'arrival times' is exactly the same as that of the subevent 'onset times', just delayed in time by a lag equal to the time it takes for the (impulsive signals emitted from all the points of an isochron) to travel the distance from the fault plane to the station. [This is why some authors (e.g. Wennerberg 1990) refer to the 'arrival times' as 'delay' or 'lag' times.] For the particular station under discussion, we can obtain an estimate of the (time-varying) normalized rate of the 'arrival times' by dividing the duration of radiation T_0 into bins, counting the subevents that ruptured over the duration of one such bin (centered at time t_k), say $n_{(t_k)}$, and dividing this number by the total number of subevents N, i.e. $\left(n_{(t_k)}/N\right)$. This procedure has been followed in preparing the corresponding histograms on the right of Fig. 4a, b. These histograms provide estimates of the PDF, $f_T\ (t)$, from which estimates of $\tilde{f}_T\ (\omega)$ may be obtained. It is evident that $f_T\ (t)$ is essentially a normalized (and time varying) rate of arrivals of pulses at the station.

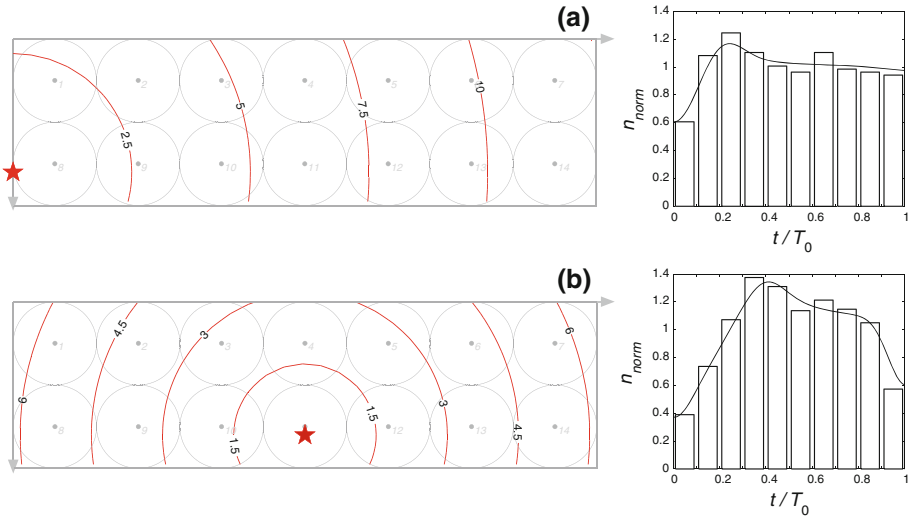

Fig. 4 The contours of the sweeping rupture front at successive time instants (1.5 s) following the initial break at the hypocenter (*star*) on a *rectangular* fault of a M_w6.5 earthquake represented by the SBM. Two rupture types are considered: unilateral (a) and bilateral (b). Also shown are the corresponding histograms of energy arrival times for far-field stations on the fault normal (in which case the contours are isochrons)

At this point we observe that selecting a different station that does not conform to the above-stated requirements, the isochrons cease to coincide with the curves describing the position of the rupture front at consecutive times, and in order to estimate the normalized rate of 'arrival times' we have to calculate and trace on the fault plane the corresponding isochrons.

Therefore, in estimating ground motion, using the source spectrum of the SBM (Eq. 10), that accounts properly for the source-station geometry, we should use the appropriate $\tilde{f}_T(\omega)$, estimated, as described above, by using the concept of the isochrons.

Solving the above-stated problem analytically is formidable, and thus we chose to proceed in a semi-empirical way. Specifically, we generated a grid of hypothetical stations surrounding earthquakes of different magnitudes, modeled by the interplate SBM (the values of the parameters that we selected are those estimated by Halldorsson and Papageorgiou (2005) who calibrated the SBM to earthquake events of three different tectonic regions): M_w5.5, with fault aspect ratio of 5 × 3 subevents (Fig. 5, top row panels); M_w6.5, with fault aspect ratio of 7 × 2 subevents (Fig. 5, middle row panels); and M_w7.5, with fault aspect ratio of 14 × 1 subevents (Fig. 5, bottom row panels). In Fig. 5, stations are denoted by triangles, and the earthquake events are assumed to take place on vertical fault planes that rupture either unilaterally (Fig. 5, right panels; the epicenter is located at the 'southern' end of the fault and propagation is towards 'north') or bilaterally (Fig. 5, left panels; the epicenter is located mid-way along the fault) For each station (j) we trace on the fault plane the corresponding isochrons, which also provide the corresponding total duration $T_0^{(j)}$ of motion at the station. We subdivided the total duration $T_0^{(j)}$ of energy arriving at each station, into bins and calculated the histogram of $\left(n_{(t_k)}/N\right)$ where N is the total number of subevents and $n_{(t_k)}$ is the number of subevents of the SBM which are contained between two successive isochrons, Δt_k seconds apart, and centered in time at t_k. The histograms obtained as described above are estimates of the PDF, $f_T^{(j)}(t)$, of pulse arrival times for station j. The individual PDFs (solid curves) are shown in Fig. 5 at their respective stations around the faults.

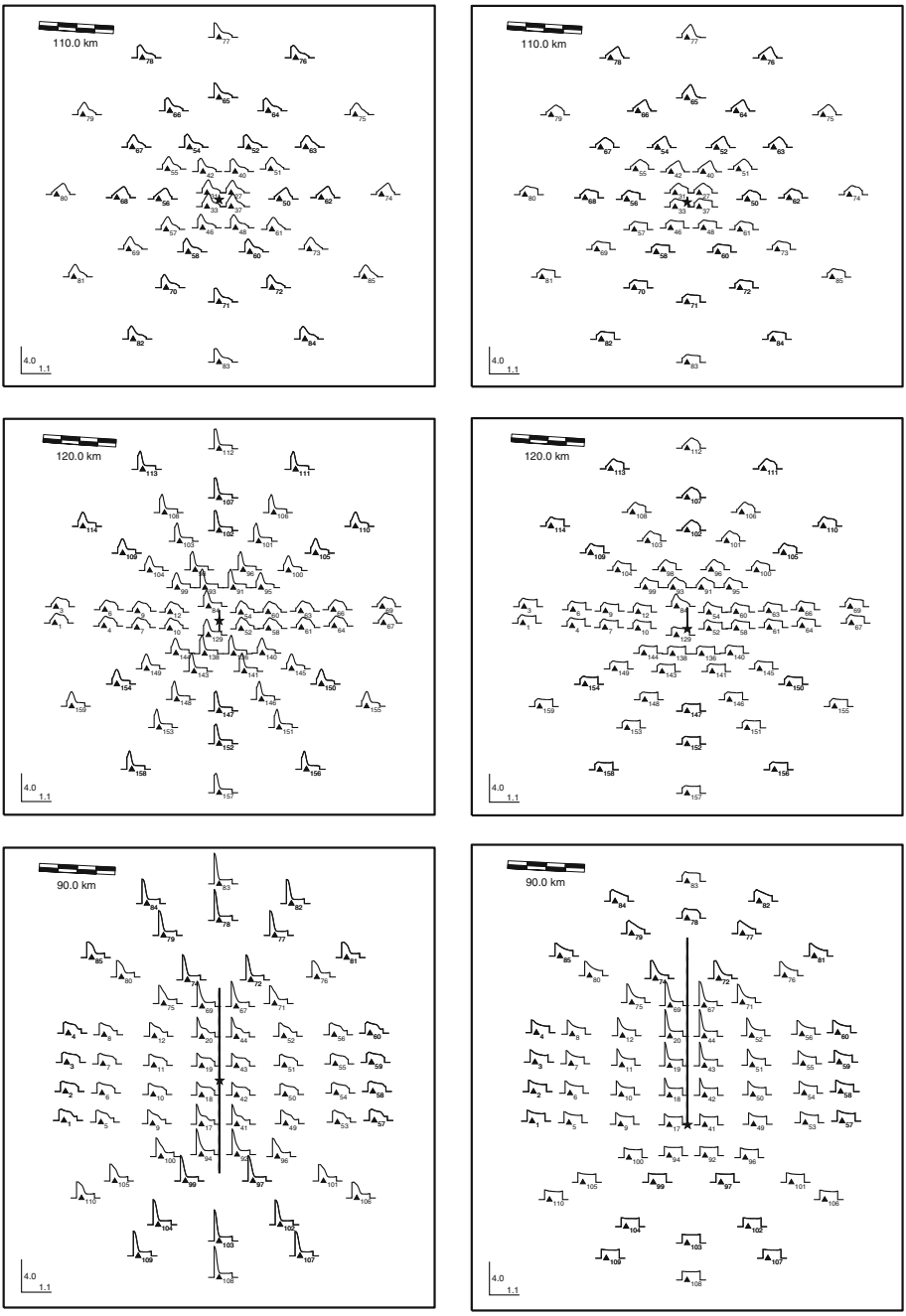

Fig. 5 The probability density functions of the energy arrival times plotted on a map of the hypothetical sites located around the SBM representing earthquakes on vertical faults of magnitudes M_w5.5, 6.5 and 7.5 (*top* to *bottom*, respectively). The PDFs are given for bilateral (*left*), and unilateral (*right*) rupture on the fault (see Fig. 4) where the star denotes the epicentral location and *the solid lines* the surface projection of the fault

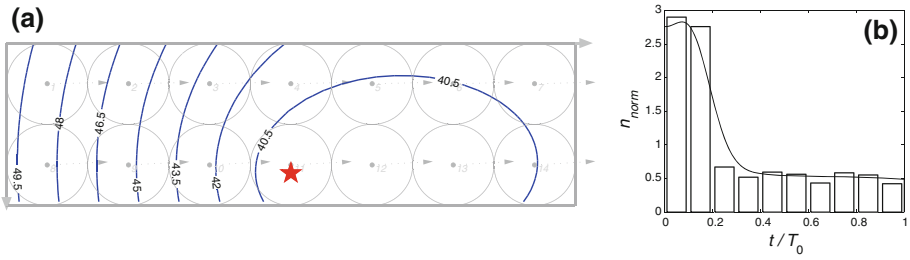

Fig. 6 **a** Isochrons contours (plotted at $\Delta t = 1.5$ s intervals) for a far-field station located on the strike of the $M_w 6.5$ earthquake on which a bilateral rupture takes place with constant rupture velocity (see Fig. 4). **b** The associated histogram and PDF of arrival times at the station. The isochrons reveal the drastic differences in the numbers of subevents from which seismic energy arrives at the station at the same time (within time interval Δt) in the first part of the strong-motion duration versus the latter parts

The results show that not all stations exhibit a constant rate of pulse arrivals. We highlight this via Fig. 6 which shows the isochrons on the fault plane corresponding to a site on the strike of the $M_w 6.5$ earthquake on which a bilateral rupture takes place (Fig. 5, left panel of middle row). At the initiation of rupture, the isochron velocity is considerably higher than in the latter part of the rupture. As a consequence, the area swept by the fast expanding isochrons at the beginning of the rupture is considerably larger as compared to the later part of the rupture. This results in a highly non-uniform pulse arrival rate, as the associated histogram and PDF shows. On the other hand, sites that experience a uniform distribution of pulse arrivals are for example the ones closest to the fault normal for $M_w 7.5$ with bilateral rupture. This is also the case for sites experiencing backward directivity from $M_w 5.5$–7.5 with unilateral rupture. On the other hand, the forward directivity stations of a unilateral rupture from $M_w 5.5$ and 6.5 experience PDFs that, in general, peak mid-way i.e., most of the pulses arriving at the sites do so near the middle of the duration. As for a unilateral rupture of the $M_w 7.5$ event, the near-fault stations experience progressively larger forward directivity effects alongside the fault, as exhibited by the growing peak in the PDFs with distance from the epicenter. Further away from the fault these effects subside. In the case of bilateral rupture however, such forward directivity effects "fan out" away from both ends of the fault and subside with sites having an increased azimuthal difference from the strike of the fault, until they more or less even out at sites close to the fault normal. However, in the direction of neutral directivity these latter sites have somewhat different distributions of arrival times than those in the case of unilateral rupture.

5 Results and discussion

For a uniform distribution on the fault plane of equal size subevents, such as that of the SBM, forward directivity is associated with high isochron velocity, with the largest part of the seismic energy arriving at the beginning of the strong-motion duration. Stations, other than those in the forward (with respect to the rupturing fault) direction, experience reduced directivity effects that gradually diminish until they reach a minimum at sites in the neutral or backward direction of rupture. The different isochron distributions on the fault plane result in PDFs of seismic energy arrival times of various shapes, depending on the geometry of the station relative to the propagating rupture front. We have classified the various PDF shapes displayed in Fig. 5 into four groups presented in Table 1, along with representative

Table 1 Summary of isochron distribution effects on the PDF of arrival times at sites, and their respective squared absolute Fourier spectra

Group:	1	2	3	4
Rupture:	Unilateral	Bilateral/Unilateral	Bilateral/Unilateral	Bilateral/Unilateral
M_w-range:	5.5 – 7.5	5.5 – 7.5 / 7.5	5.5 – 6.5 / 5.5 – 6.5	5.5 – 7.5 / 5.5 – 7.5
Field:	FF+NF	NF / FF	FF / FF	FF+NF / NF
Directivity:	BD+ND	ND / FD	ND / FD	FD / FD

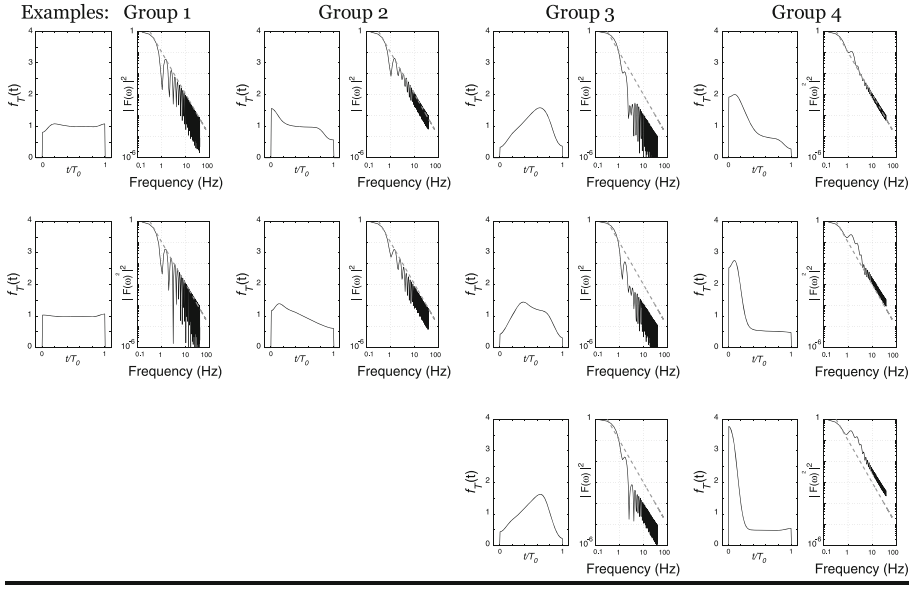

far-field *FF*, near-fault *NF* region, backward *BD*, neutral *ND* and forward *FD* directivity

PDF shapes for each group. They are characterized by directivity, proximity to the fault (i.e., near-fault versus far-field), type of rupture and magnitude range. The corresponding squared Fourier amplitude spectra (FAS) of the PDFs, $\left|\tilde{f}_T^{(j)}(\omega)\right|^2$, are also shown in Table 1, since it is through $\left|\tilde{f}_T^{(j)}(\omega)\right|^2$ the FAS that the source spectra of the SBM are affected in Eq. (10). [We note however, the analysis and Eqs. (4) and (10) are strictly speaking valid only at the far-field. Therefore, only the PDFs at far-field sites (considered here to be at distances larger than one source dimension) are considered for application to construct the earthquake source spectrum corresponding to a given source-station geometry].

While the PDF shapes in the first two groups differ, the spectral levels are very similar to that of the uniform distribution (the dashed lines indicate the spectral slope of the FASs of group 1). Therefore, the assumption of the uniform-PDF may (as an acceptable approximation) be valid for the corresponding source-site geometries i.e., those experiencing backward and neutral directivity effects in the far-field region of unilateral rupture on faults of M_w5.5–7.5. Also, sites in the far-field and forward direction from a unilateral rupture on a M_w7.5 fault, as well as near-fault sites of a bilateral rupture on faults of M_w5.5–7.5 experiencing neutral directivity. However, the assumption of uniform PDF is not valid in the cases shown in the last two colums in Table 1. That would include the far-field sites experiencing neutral and forward directivity effects from a bidirectional and unidirectional, respectively, rupture on faults of M_w5.5–6.5. As expected, the most intense forward directivity effects would

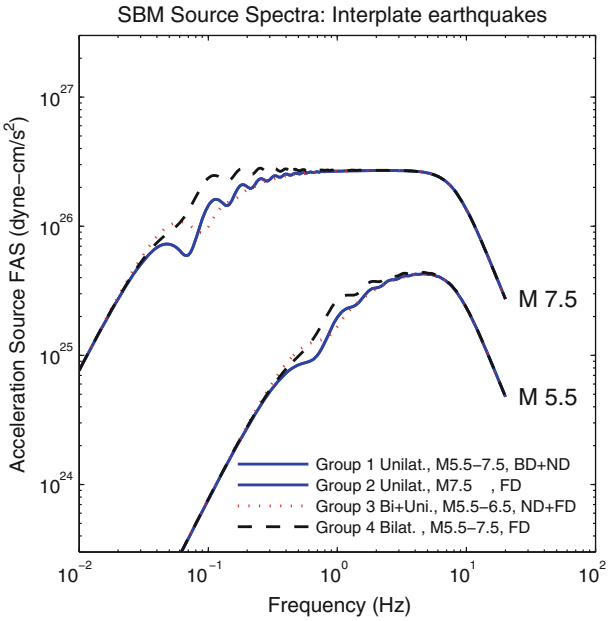

Fig. 7 The far-field source acceleration FAS of the interplate specific barrier model for M_w5.5 and 7.5 and each of the four groups of PDF shapes that depend on directivity effects from the finite-fault SBM. The first two groups have effectively the same squared FAS of energy arrival times and have therefore been grouped together

be experienced by near-fault sites of a unilateral rupture. Near-fault and far-field sites of a bilateral rupture, on faults of M_w5.5–7.5, even though they display a similar shape for $f_T\ (t)$ as the one in the case of unilateral rupture, may not experience forward directivity with the same intensity if the subevents do not rupture symmetrically.

The spectra associated with the last two groups of Table 1 reveal that the spectral levels and corner frequencies can be quite different from those displayed in the first two groups. As we have shown, the spectral characteristics of the subevent signal arrival times affect the aggregate spectrum mainly at the intermediate frequencies. The extent of the effect in turn depends on magnitude (i.e., over what frequency range the intermediate-part is), and the stress-drop ratio $\Delta\sigma_L/\Delta\sigma_G$ (with decreasing stress-drop ratio, the aggregate spectra approaches the "*ω-square*" spectrum; see Part I). In any case, for stations which are associated with strongly non-uniform PDFs, $f_T\ (t)$, of pulse arrival times, it is more consistent to use the corresponding $\tilde{f}_T\ (\omega)$ in the source spectrum expressed by Eq. (10).

We take advantage of the grouping in Table 1 for the estimation of directivity effects on the SBM far-field spectra. For each group we calculate the average of the representative PDFs and approximate it using a simple functional form (polynomials of the appropriate order), for which we calculate the squared FAS and present in closed form (see "Appendix"). The effects of the four groups of PDF shapes on the acceleration source FAS are summarized in Fig. 7. The figure shows the far-field SBM source spectrum $S(M_\circ, f, \zeta)$ in Eq. (4) for interplate earthquakes ($s_m = -0.12$, $M_c = 6.35$) for two magnitudes, M_w5.5 and 7.5. Note that the spectra are shown with high-frequency $f_{\max}$-diminution effects as in Fig. 1b. The spectra shown by solid lines are associated with a uniform distribution of energy arrival times (Halldorsson and Papageorgiou 2005, which can be thought to correspond to the PDFs in the first two groups of Table 1. Although the second group PDF shapes are not constant,

the effects on the spectra are effectively the same as those of a uniform distribution. On the other hand, the spectra shown by dotted and dashed lines correspond to the PDFs of arrival times in groups 3 and 4, respectively. We observe that stations receiving directivity effects of the form associated with group four in the table have higher spectral levels at intermediate-frequencies when compared to the spectra associated with a uniform distribution. This difference becomes greater with magnitude.

As we have noted, the relative effects associated with the different arrival time distributions only affect the intermediate frequency levels according to the formulation on which the current analysis is based. In terms of source strength the high-frequency spectral levels of the SBM are controlled by the stress drops ($\sim \Delta\sigma_L \Delta\sigma_G^{-1/3}$), both of which have been shown to be constant for earthquakes in a given tectonic region (Halldorsson and Papageorgiou 2005). Additionally however and unrelated to the source strength, if the site is in the forward direction the higher isochron velocity on the fault manifests itself in strong-motion of shorter duration and higher relative amplitude, as opposed to a site in the backward direction experiencing relatively lower amplitudes of strong-motion over a longer duration. Consequently, while the source spectrum may show similar *high*-frequency spectral levels at the two sites (see Fig. 7), the high-frequency spectral levels of the *site*-spectrum will be higher for the site in the forward direction compared to the site in the backward direction. This feature has not yet been incorporated into the current result.

6 Conclusions

An expression of the far-field source spectrum radiated from a realistic, yet simple composite earthquake source model, such as the SBM, can be useful for expedient simulations of seismic ground motions using the stochastic modeling approach. While the high-frequency source spectral levels can be affected by the statistical characteristics of the subevent population (see Part I), the shape of the spectrum of such a composite earthquake source at intermediate-frequencies is however largely affected by the shape of $|\tilde{f}_T(\omega)|^2$. In the past, the PDF $f_T(t)$ had been assumed to be constant (i.e., uniform distribution of 'arrival times'). While a uniform distribution of 'arrival times' is the simplest assumption, it is not necessarily valid for all source-station geometries. We have seen that the $f_T(t)$ depends on the source-site geometry and on the evolution of the rupture front. Both these factors are captured effectively by the isochrons curves. By postulating different earthquake scenarios on vertical finite-size faults, modeled using the SBM, and considering two different rupture modes (fault rupture is associated with a circular rupture front spreading with constant velocity), isochrons have been constructed corresponding to each station of a grid of stations surrounding the causative fault. The PDFs of pulse arrival times at each station was estimated using the corresponding isochrons. Classifying the stations based on the shape of $f_T(t)$, we obtained four groups of stations. In general, stations in the forward (w.r.t. the advancing rupture) direction are observed to have higher spectral levels at intermediate frequencies as compared with those at other sites. This is attributed to the higher 'arrival rate', especially at the beginning of the duration of radiation.

The analysis presented in this paper, along with that of Part I, generalize the SBM originally proposed by Papageorgiou and Aki (1983a). These companion studies demonstrate that while relaxation of certain key assumptions of the SBM introduces variations in the source spectra, these variations are such that allow us to continue using the SBM in its original form as an unbiased benchmark for ground motion analysis and simulation.

Acknowledgments This work was supported by Contract Numbers MCEER 00-0102, 01-0102, 02-0102, 03/0.1, and 04-0001 under the auspices of the Multidisciplinary Center for Earthquake Engineering Research (MCEER), Buffalo, New York; the United States National Science Foundation, Award Number EEC-9701471; the Icelandic Centre for Research (RANNIS) Project Grants No. 60043021, 90049021/22/23. The calculations were carried out in Scientific WorkPlace and Matlab. The authors are grateful to the anonymous reviewers for comments that improved this paper.

Appendix

Equations for approximating general shapes of arrival times PDFs

PDF shapes of group 1 of Table 1 are approximated by Eq. (11) and the corresponding squared absolute Fourier spectrum is given by Eq. (12).

The average shape of the representative PDF functions in group 2 of Table 1 is approximated by a straight line

$$f(t) = at + b, \quad t \in [0; T_0] \tag{13}$$

where the following parameters

$$a = -10^{-1.9998 \log T_0 - 0.1009} \tag{14}$$

$$b = 10^{-\log T_0 + 0.1458} \tag{15}$$

ensure that the PDF has an area of unity over a range of realistic values of T_0. The simple functional form of the PDF enables a concise closed form expression of the corresponding squared Fourier amplitude spectrum:

$$\left|\tilde{f}_T(\omega)\right|^2 = \frac{-4}{T_0^2\omega^4(2b + T_0a)^2}\left(\left(2a^2 + 2T_0ab\omega^2 + 2b^2\omega^2\right)\cos(T_0\omega) + 2T_0a^2\omega\sin(T_0\omega) - 2T_0ab\omega^2 - 2a^2 - 2b^2\omega^2 - T_0^2a^2\omega^2\right) \tag{16}$$

In the same way, the average shape of the representative PDF functions in group 3 of Table 1 are approximated by a simple function, in this case a 2nd degree polynomial

$$f(t) = at^2 + bt + c \quad , \quad t \in [0; T_0] \tag{17}$$

with the following parameters

$$a = -10^{-3 \log T_0 + 0.7} \tag{18}$$

$$b = 10^{-2 \log T_0 + 0.709} \tag{19}$$

$$c = 10^{-\log T_0 - 0.95} \tag{20}$$

The corresponding squared absolute Fourier spectrum is

$$\left|\tilde{f}_T(\omega)\right|^2 = \frac{1}{\omega^6}(8a^2 + \omega^2(2b^2 - 8ac) + \omega^4(2T_0bc + 2c^2 + 2T_0^3ab + T_0^4a^2 + T_0^2(2ac + b^2)) + \sin(T_0\omega)(\omega^3(4T_0ac - 2T_0b^2 - 2T_0^2ab) - 8T_0a^2\omega) - 2\cos(T_0\omega)(4a^2 + \omega^4(T_0bc + c^2 + T_0^2ac) + \omega^2(b^2 - 4ac - 2T_0^2a^2))) \tag{21}$$

Similarly, the average shape of the representative PDF functions in group 4 of Table 1 are approximated by a 3rd degree polynomial

$$f(t) = at^3 + bt^2 + ct + d \quad , \quad t \in [0; T_0] \tag{22}$$

with the following parameters

$$a = -10^{-3.9967 \log T_0 + 0.8941} \tag{23}$$
$$b = 10^{-2.9960 \log T_0 + 1.2323} \tag{24}$$
$$c = -10^{-1.9957 \log T_0 + 1.0881} \tag{25}$$
$$d = 10^{-0.9978 \log T_0 + 0.5318} \tag{26}$$

The corresponding squared absolute Fourier spectrum is

$$\begin{aligned}\left|\tilde{f}_T(\omega)\right|^2 = &\left(\frac{1}{\omega^8}\right)\left(72a^2 + 8\omega^2\left(b^2 - 3ac\right)\right.\\ &+\omega^4\left(2c^2 - 12T_0ad - 8bd - 6T_0^6ac - 4T_0^3ab - 3T_04a^2\right)\\ &+\omega^6(2T_0cd + 2d^2 + 2T_0^5ab + T_0^6a^2 + T_0^4\left(2ac + b^2\right)\\ &\left.+T_0^2\left(2bd + c^2\right) + 2T_0^3\left(ad + bc\right)\right)\\ &+\left(\frac{1}{\omega^8}\right)\sin\left(T_0\omega\right)\left(24T_0ac\omega^3 - 72T_0a^2\omega + 4T_0bd\omega^5\right.\\ &-8T_0b^2\omega^3 - 2T_0c^2\omega^5 + 6T_0^2ad\omega^5 - 2T_0^2bc\omega^5 - 2T_0^3ac\omega^5\\ &\left.+12T_0^3a^2\omega^3\right) + \left(\frac{1}{\omega^8}\right)\cos T_0\omega(24acw^2 - 72a^2 + 8bd\omega^4\\ &+12T_0ad\omega^4 - 2T_0cd\omega^6 - 8b^2\omega^2 - 2c^2\omega^4 - 2d^2\omega^6\\ &-6T_0^2ac\omega^4 + 4T_0^3ab\omega^4 - 2T_0^2bd\omega^6 - 2T_0^3ad\omega^6\\ &+36T_0^2a^2\omega^2 + 4T_0^2b^2\omega^4)\end{aligned} \tag{27}$$

References

Aki K (1967) Scaling Law of seismic spectrum. J Geophys Res 72(4):1217–1231

Aki K, Papageorgiou AS (1988) Separation of source and site effects in acceleration power spectra of major California earthquakes. In: Proceedings of the 9th world conference on Earthquake Engingeering, pp 163–165

Aki K, Richards PG (1980) Quantitative seismology. Theory and methods. W. H. Freeman and Company, San Francisco

Davenport WB (1970) Probability and random processes: an introduction for applied scientists and engineers. McGraw-Hill, New York

Douglas J (2010) Consistency of ground-motion predictions from the past four decades. Bull Earthq Eng 8(6):1515–1526

Eshelby JD (1957) The determination of the elastic field of an ellipsoidal inclusion, and related problems. Proc R Soc Lond Ser A Math Phys Sci 241(1226):376–396

Foster KM, Halldorsson B, Green RA, Chapman MC (2012) Calibration of the specific barrier model to the NGA dataset. Seism Res Lett (in press)

Frankel A (1991) High-frequency spectral falloff of earthquakes, fractal dimension of complex rupture, b value, and the scaling of strength on faults. J Geophys Res 96(B4):6291–6302

Gusev AA (1983) Descriptive statistical model of earthquake source radiation and its application to an estimation of short-period strong motion. Geophys J R Astron Soc 74(3):787–808

Halldorsson B, Mavroeidis GP, Papageorgiou AS (2011) Near-fault and far-field strong ground motion simulation for earthquake engineering applications using the specific barrier model. J Struct Eng 137(3): 433–444
Halldorsson B, Ólafsson S, Sigbjörnsson R (2007) A fast and efficient simulation of the far-fault and near-fault earthquake ground motions associated with the june 17 and 21, 2000, earthquakes in South Iceland. J Earthquake Eng 11(3):343
Halldorsson B, Papageorgiou AS (2005) Calibration of the specific barrier model to earthquakes of different tectonic regions. Bull Seismol Soc Am 95(4):1276–1300
Halldorsson B, Papageorgiou AS (2012) Variations of the specific barrier model—part I: effect of subevent size distributions. Bull Earthq Eng. doi:10.1007/s10518-012-9344-0
Housner GW (1947) Characteristics of strong-motion earthquakes. Bull Seismol Soc Am 37(1):19
Housner GW (1955) Properties of strong ground motion earthquakes. Bull Seismol Soc Am 45(3):197–218
Joyner WB, Boore DM (1986) On simulating large earthquakes by Green's function addition of smaller earthquakes. In: Das S (ed) Earthquake source mechanics. Maurice Ewing series. American Geophysical Union, Washington, pp 269–274
Keilis-Borok VI (1959) On the estimation of the displacement in an earthquake source and of source dimensions. Ann Geo 12:205–214
Lin YK (1967) Probabilistic theory of structural dynamics. McGraw-Hill, New York
Lin YK, Cai G-Q (1995) Probabilistic structural dynamics: advanced theory and applications. McGraw-Hill Professional, New York
Mavroeidis GP, Papageorgiou AS (2003) A mathematical representation of near-fault ground motions. Bull Seismol Soc Am 93(3):1099–1131
Middleton D (1960) An introduction to statistical communication theory 1987th edn. McGraw-Hill, New York
Papageorgiou AS (1988) On two characteristic frequencies of acceleration spectra: patch corner frequency and fmax. Bull Seismol Soc Am 78(2):509–529
Papageorgiou AS (2003) The barrier model and strong ground motion. Pure App Geophy 160(3):603–634
Papageorgiou AS, Aki K (1983a) A specific barrier model for the quantitative description of inhomogeneous faulting and the prediction of strong ground motion. I. Description of the model. Bull Seismol Soc Am 73(3):693–722
Papageorgiou AS, Aki K (1983b) A specific barrier model for the quantitative description of inhomogeneous faulting and the prediction of strong ground motion. Part II. Applications of the model. Bull Seismol Soc Am 73(4):953–978
Papageorgiou AS, Aki K (1985) Scaling law of far-field spectra based on observed parameters of the specific barrier model. Pure Appl Geophys 123(3):353–374
Papoulis A (1965) Probability, random variables, and stochastic processes. McGraw-Hill, New York
Rice SO (1944) Mathematical analysis of random noise. Bell Syst Tech J 23:282–332
Rice SO (1945) Mathematical analysis of random noise. Bell Syst Tech J 24:46–156
Sato T, Hirasawa T (1973) Body wave spectra from propagating shear cracks. J Phys Earth 21:415–431
Silver P (1983) Retrieval of source-extent parameters and the interpretation of corner frequency. Bull Seismol Soc Am 73(6A):1499–1511
Spudich P, Frazer LN (1984) Use of ray theory to calculate high-frequency radiation from earthquake sources having spatially variable rupture velocity and stress drop. Bull Seismol Soc Am 74(6):2061–2082
Trifunac MD, Brune JN (1970) Complexity of energy release during the Imperial Valley, California, earthquake of 1940. Bull Seismol Soc Am 60(1):137–160
Vallée M, Bouchon M (2004) Imaging coseismic rupture in far field by slip patches. Geophys J Int 156(3):615–630
Wennerberg L (1990) Stochastic summation of empirical Green's functions. Bull Seismol Soc Am 80(6A):1418–1432
Wyss M, Brune JN (1967) The Alaska earthquake of 28 March 1964: a complex multiple rupture. Bull Seismol Soc Am 57(5):1017–1023